Generalisable Relational Reasoning With Comparators in Low-Dimensional Manifolds

Duo Wang[*] **Mateja Jamnik** **Pietro Lio**

Department of Compute Science and Technology, University of Cambridge
Cambridge, UK, CB3 0FD

Abstract

While modern deep neural architectures generalise well when test data is sampled from the same distribution as training data, they fail badly for cases when the test data distribution differs from the training distribution even along a few dimensions. This lack of out-of-distribution generalisation is increasingly manifested when the tasks become more abstract and complex, such as in relational reasoning. In this paper we propose a neuroscience-inspired inductive-biased module that can be readily amalgamated with current neural network architectures to improve out-of-distribution (o.o.d) generalisation performance on relational reasoning tasks. This module learns to project high-dimensional object representations to low-dimensional manifolds for more efficient and generalisable relational comparisons. We show that neural nets with this inductive bias achieve considerably better o.o.d generalisation performance for a range of relational reasoning tasks. We finally analyse the proposed inductive bias module to understand the importance of lower dimension projection, and propose an augmentation to the algorithmic alignment theory to better measure algorithmic alignment with generalisation.

1 Introduction

The goal of Artificial Intelligence research, first proposed in the 1950s and reiterated many times, is to create machine intelligence comparable to that of a human being. While today's deep-learning-based systems achieve human-comparable performances in specific tasks such as object classification and natural language understanding, they often fail to generalise when the test data distribution differs from the training data distribution [33, 40, 4, 6]. Moreover, it is observed that the generalisation error increases as the tasks become more abstract and require more reasoning than perception. This ranges from small drops (3% to 15%) in classification accuracy on ImageNet [33] to accuracy only slightly better than random chance for the Raven Progressive Matrices (RPM) test (a popular Human IQ test), when testing data are sampled completely out of the training distribution [4].

In contrast, human brain is observed to generalise better to unseen inputs [13], and typically requires only a small number of training samples. For example, a human, when trained to recognise that there is a progression relation of circle sizes in Figure 1a, can easily recognise that the same progression relation exists for larger circles in Figure 1b, even though such size comparison has not been done between larger circles. However, today's state-of-the-art neural networks [4, 43] are not able to achieve the same. Researchers [37, 10, 5, 45] argue that the human brain evolved to develop special inductive-biases that adapt to the form of information processing needed for humans, thereby improving generalisation. Examples include convolution-like cells in the visual cortex [21, 17] for

[*]Correspondence to Duo Wang (duo.wang@cl.cam.ac.uk).

Preprint. Under review.

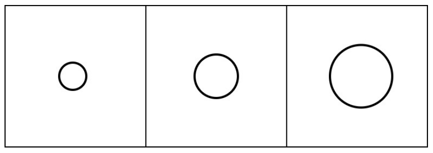
(a) Small Circles

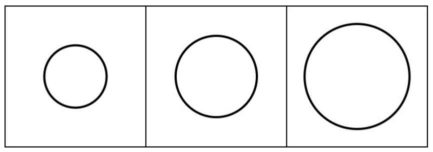
(b) Big Circles

Figure 1: Size Progression Relations for circles of different sizes.

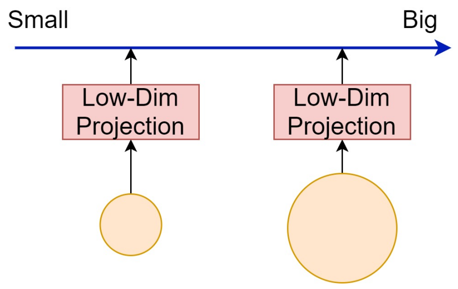

Figure 2: Illustration of projecting object representations onto a 1-dimensional manifold in which size comparison can be achieved by simply measuring the difference between two projections.

visual information processing, and grid cells [18] for spatial information processing and relational comparison between objects [5].

In this work, we propose a simple yet effective inductive bias which improves generalisation for relational reasoning. This inductive-bias is inspired by neuroscience and psychology research [12, 9, 39] showing that in primate brain there are neurons in the Parietal Cortex which only responds to different specific attributes of perceived entities. For examples, certain LIP neurons fire at higher rate for larger objects, while the firing rate of other neurons correlates with the horizontal position of objects in the scene (left vs right) [14]. From a computational perspective, this can be viewed as projecting object representations to low-dimensional manifolds. Based on these observations [39], we hypothesise that these neurons evolved to learn low-dimensional representations of relational structure that are optimised for abstraction and generalisation, and the same inductive bias can be readily adapted for artificial neural network to achieve similar optimisation for abstraction and generalisation.

We test this hypothesis by designing an inductive bias module which projects high-dimensional object representations into low-dimensional manifolds, and make comparisons between different objects in these manifolds. We show that this module can be readily amalgamated with existing architectures to improve out-of-distribution generalisation performance for different relational reasoning tasks. Specifically, we performed experiments on three different out-of-distribution generalisation tasks, including maximum of a set, visual object comparison on dSprites dataset [20] and extrapolation on Progressive Generated Matrices [4]. We show that models with the proposed low-dimensional comparators perform considerably better than baseline models on all three tasks. In order to understand the effectiveness of comparing in low-dimensional manifolds, we analyse the projection space and corresponding function space of the comparator to show the importance of projection to low-dimensional manifolds in improving generalisation. Finally we perform analysis relating to algorithmic alignment theory [45], and propose an augmentation to the sample complexity criteria used by this theory to measure algorithmic alignment to better measure algorithmic alignment with generalisation.

This paper makes the following major contributions:

- We propose a neuroscience-inspired inductive-bias which can be readily amalgamated with existing neural network architectures to achieve improved out-of-distribution generalisation performance on relational reasoning tasks.
- We analyse the low-dimensional projection space and corresponding function space of the comparator to shed light on the effectiveness of comparison in lower dimensional manifolds.
- We propose an augmentation to the sample complexity criteria used in algorithmic alignment theory to better measure algorithmic alignment with consideration on generalisation.

2 Method

Here, we describe the inductive bias module we developed to test our hypothesis that the same inductive bias of low-dimensional representation observed in Parietal Cortex can be readily adapted for artificial neural network to achieve similar optimisation for abstraction and generalisation. The proposed module learns to project object representations into low-dimensional manifolds and make comparisons in these manifolds. In Section 2.1 we describe the module in details. In Section 2.2, 2.3 and 2.4 we discuss how this module can be utilised for three different relational reasoning tasks, which are finding the maximum of a set, visual object comparisons and Raven Progressive Matrics (RPM) reasoning.

2.1 Comparator in Low-Dimensional Manifolds

The inductive-bias module is comprised of low-dim projection functions p and comparators c. Let $\{o_i; i \in 1 \ldots N\}$ be the set of object representations, obtained by extracting features from raw inputs such as applying Convolutional Neural Networks (CNN) on images. Pairwise comparison between object pair o_i and o_j can be achieved with a function f expressed as:

$$f(o_i, o_j) = g(\mathop{||}_{k=1}^{K} c_k(p_k(o_i), p_k(o_j))). \tag{1}$$

Here p_k is the k^{th} projection function that projects object representation o into the k^{th} low dimensional manifold, c_k is the k^{th} comparator function that compares the projected representations, $||$ is the concatenation symbol and g is a function that combines the K comparison results to make a prediction. Having K parallel projection functions p_k and comparators c_k allows simultaneous comparison between objects with respect to their different attributes. Figure 2 shows an example of comparing sizes of circles by projection onto a 1-dimensional manifold. Both p and c can be implemented as feed forward neural networks. While the comparator c, implemented as neural network, can theoretically learn a rich range of comparison metrics. We found that adding to c an additional inductive-bias of distance measure for the projection, such as vector distance $p(o_i) - p(o_j)$ or absolute distance $|p(o_i) - p(o_j)|$, improves generalisation performance.

Let $a_t(o_i)$ be the ground truth mapping function from i^{th} object's representation o_i to its t^{th} attributes (such as colour and size for a visual object). If such ground truth labels of object attributes exist, $f(o_i, o_j)$ can be trained to directly predict the differences in attributes by minimising the loss $\mathcal{L}(d(a_t(o_i), a_t(o_j)), f(o_i, o_j))$, where d is a distance function (*e.g.*, $a_t(o_i) - a_t(o_j)$ for continuous attributes or $\mathbb{1}_{a_t(o_i)=a_t(o_j)}$ for categorical attributes). However, in real-world datasets, such ground truth attribute labels seldom exist. Instead, in many relational reasoning tasks, learning signals for attribute comparison are only provided implicitly in the training objective. For example, in Visual Question Answering task, an example question might be 'Is the object behind Object A smaller?'. The learning signals for the required size and spatial position comparator is provided only through correctness of the answers to the given questions. Thus, the proposed module is only useful and scalable if it can be integrated into neural architectures for relational reasoning and still learn to compare attributes with the weaker, implicit learning signal. Next, we describe 3 examples of such integrations for different relational reasoning tasks, and show in Section 3 that the proposed module can learn relational reasoning tasks with better generalisation capability.

2.2 Architecture: Maximum of a set

The first task we consider is finding the maximum of a set of real numbers. Formally, given a set $\{x_i; i \in 1 \ldots N\}$ where x_i is a real number represented as a scalar value, we want to train a function $h_{max}(\{x_i, \ldots, x_N\})$ that gives the maximum value in the set. Many neural architectures have been applied on this task, including Deep Sets [47] and Set Transformer [27], but none of them test the out-of-distribution (**o.o.d**) generalisation capability. In order to test **o.o.d** generalisation, we create the training and test such that their ranges do not overlap. We sample from the range $(V_{low}^{train}, V_{high}^{train})$ for the training set, and from the range $(V_{low}^{test}, V_{high}^{test})$ for the test set, and restrict that $V_{high}^{train} < V_{low}^{test}$.

We integrate the proposed low-dim comparator module with Set Transformer [27], a state-of-the-art neural architecture for sets. Set Transformer first encodes each element in the set with respect to all other elements with a Multihead Attention Block (MAB), an attention module modified from self-attention used in language tasks [41]): $e_i = encode(x_i) = \mathsf{MAB}(x_i, x_j)$. The Set Transformer then uses Pooling with Multihead Attention to combine all encoded elements of the set as $\mathsf{PMA}(e_1, \ldots, e_N)$. While MAB use query and key embeddings to generate attention variables, which are then used as weights in the weight sum of value embeddings of elements, we swap the query-key attention mechanism with our low-dim comparator as:

$$e_i = MLP(\sum_{j=1}^{N} f(x_i, x_j)) \tag{2}$$

Here f is the low-dim comparator and MLP is a standard Multi-Layer Perceptron. Note that we directly use the scalar input x_i as object representation o_i in Equation (1) as no feature extraction is needed. We then use attention-based pooling to combine projection of x_i as $\sum_{i=1}^{N} a(e_i)p(x_i)$, where a output attention values while p is the 1-dim projection function. For detailed architecture configuration, please refer to Appendix A.

2.3 Architecture: Visual Object Comparison

The second task we consider is comparing visual objects for different attributes such as size and spatial position. For this task, two images x_1 and x_2 containing single objects of randomly sampled attributes are given, and one is asked if a specific attribute of the second object is larger than, equal to, or smaller than the attribute of the first object. Figure 3a shows an example of this task for comparing sizes between two heart-shaped objects. For implementation, we used dSprites dataset [20], a widely used dataset for studying latent space disentangling, to sample images of objects. To test out-of-distribution generalisation, we sample training set and test set such that for the compared attribute, the training attribute range has no overlap with the test attributes. We leave details of the dataset construction to Appendix B.

Figure 3a shows an overview of the architecture integrated with the proposed low-dimensional comparator. The image pair x_1 and x_2 is first passed through a CNN to extract feature embeddings e_1 and e_2. The feature embeddings are then projected to low-dim manifold and compared as $c(p(e_1), p(e_2))$, where p is the projector and c is the comparator. The comparator has 3 output units with softmax to predict probabilities that an attribute of the second object $a(x_2)$ is smaller than, equal to, or larger than the attribute of the first object $a(x_1)$. The architecture is trained with cross entropy loss with respect to ground truth labels. While we are testing the o.o.d generalisation of relational reasoning, it is reasonable to expect that the visual perception module is exposed to all possible scenarios of the input distribution in an unsupervised way. The same assumption also holds for humans, whose vision system has to be exposed to the world inputs sufficiently after birth before they can associate objects with semantic meaning and perform relational reasoning [32]. Thus, we initialise the CNN with the pretrained encoder weights of Beta-VAE [20], a disentangled VAE model trained in the unsupervised setup on dSprites dataset. For detailed configuration of the architecture please refer to Appendix C.

2.4 Architecture: Visual Reasoning for Raven Progressive Matrices

The third task we consider is a more complex visual reasoning task named 'Raven Progressive Matrices' (RPM), which is a popular human IQ test. In this task one is given 8 context diagrams with logic relations present in them, and is asked to pick an answer that best fits with the context diagrams. In this experiment we use the PGM dataset [4], the largest RPM-style dataset available. In PGM dataset, there is a special data split called 'extrapolation' which is designed to test for **o.o.d** generalisation.

In this split, colour and size values of objects in the training set are sampled from the lower half of the range, while the same attributes in test set are sampled from the upper half of the range. Thus the attribute ranges of training and test set are non-overlapping. For details and examples of PGM dataset, please refer to Appendix D or Barrett et al [4].

Our architecture integrates the low-dim comparator with a Multi-Layer Relation Network [22]. Figure 3b shows an overview of the architecture developed for PGM tasks. We use a 2-layer relation network with the first layer encoding pairs of diagrams within a row/column and the second layer encoding pairs of rows/columns. Applying such prior knowledge that rules only exist in rows and columns has been standard practice in state-of-the-art methods for RPM reasoning [43, 48]. Following [43] we fill each of the 8 candidate answers to the third row and columns to obtain in total 16 answer row and columns. At each layer of the relation network, we use the low-dimensional comparator instead of the MLP in the original relation network [36] for diagram comparison. Diagram

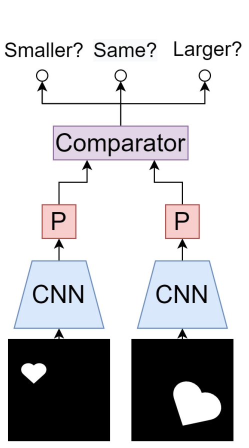

(a) dSprites

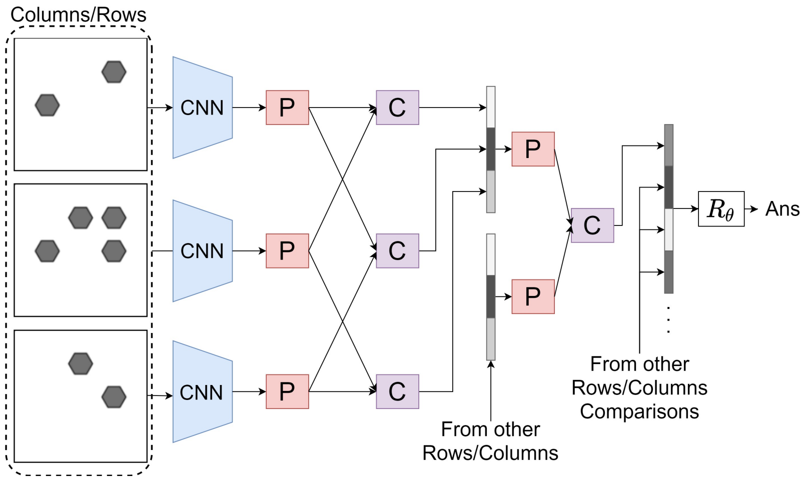

(b) RPM

Figure 3: Figure (a) illustrates the architecture for comparing sizes of objects sampled from dSprites dataset. "P" is the projection function. Figure (b) illustrates the architecture for logical reasoning on RPM-style tasks. "P" is the projection function and "C" is the comparator (g in Equation 1).

x_i is first passed through a CNN to produce embedding o_i. embedding pairs (o_i, o_j) are then compared as $e_{ij} = f(o_i, o_j)$, where f is the low-dimensional comparator described in Equation (1). Comparison results from the same row/columns are then concatenated to form row/column embedding $r_{ijk} = e_{ij}||e_{ik}||e_{jk}$. The row/column embeddings are compared with the second layer comparator. The comparison results are then concatenated and input into a reasoning network R_θ to predict the correct answer. Similar to dSprites comparison task, as discussed in Section 2.3, we pre-train CNN as encoders of VAE, a technique that has also been previously explored for PGM dataset [38]. For detailed configuration of the architecture please refer to Appendix E.

2.5 Algorithmic Alignment and o.o.d Generalisation

Xu et al [45] proposed to measure algorithmic alignment of neural networks to a specific task with sample complexity $\mathcal{C}_\mathcal{A}(g, \epsilon, \delta)$, which is the minimum sample size M so that g, the ground truth label mapping function, is (M, ϵ, δ) learnable with a learning algorithm $\mathcal{A}$. This essentially says that a model is more algorithmically aligned with a task if it can learn the task more easily with fewer samples. However, in the original definition, both training and test data are independently and identically distributed (i.i.d) samples drawn from the same data distribution. Thus the algorithmic alignment theory measures how well can a NN fit to a particular data distribution, but does not measure how well can a NN model perform in the **o.o.d** scenario. For example, for the visual object comparison task, an over-parameterised MLP can learn the following two algorithms with low complexity: (1) $m(hash(o_i), hash(o_j))$ where $hash$ is a hashing function and m is a memory read/write function based on the hash index; (2) $c(p(o_i), p(o_j))$ which is our proposed comparator function. While both algorithms can fit well for the training data, the first algorithm clearly does not **o.o.d** generalise as the memory function does not store unseen samples. In Section 3.5 we also show by experiments that algorithmic alignment is not indicative of **o.o.d** generalisation.

Intuitively, a more algorithmically aligned model should generalise better as it captures better the underlying algorithm of label generation. Here we propose an augmentation to sample complexity metric (Definition 3.3 in Xu et al [45]) in order to measure for algorithmic alignment with generalisation.

Definition 2.1. o.o.d metric. Fix an error parameter $\epsilon > 0$ and failure probability $\delta \in (0, 1)$. Suppose $\{x_i^s, y_i^s\}_{i=1}^M$ are i.i.d samples from distribution $\mathcal{D}_s = \mathcal{T}(\mathcal{D}, \beta, \mathbf{u})$, where $\mathcal{D}$ is the full data distribution, $\mathcal{T}$ is a truncating function, $\beta \in (0, 1)$ is the truncation ratio, and $\mathbf{u}$ is the set of dimensions for truncation. Let g be the underlying data function $y_i = g(x_i)$, and $f = \mathcal{A}(\{x_i, y_i\}_{i=1}^M)$ be the function learnt with learning algorithm $\mathcal{A}$. Then g is $(M, \epsilon, \delta, V, \beta, \mathbf{u}) - learnable$ with $\mathcal{A}$ if:

$$\mathbb{P}_{x \sim \mathcal{D}}[||f(x) - g(x)|| < \epsilon] \geq 1 - \delta \quad (3)$$

The sample complexity is the minimum M for g to be $(M, \epsilon, \delta, V, \beta, \mathbf{u}) - learnable$ with $\mathcal{A}$. In Section 3.5 we show experimentally that this metric measures better a NN's ability to generalise.

3 Evaluation

3.1 Maximum of a set

For the task of finding the maximum number in a set, we randomly sample number sets of cardinality ranging from 2 to 20 for training, and 2 to 40 for testing. For number sets for training, we uniformly sample numbers in the real value range $[0, 100)$. For testing we sample numbers in the range $[100, 200]$. In this way we both test if the model can generalise for sets of larger cardinality and for numbers sampled from unseen range. We sampled 10000 sets for training and 2000 sets for testing. For hyper-parameters of this and subsequent experiments please refer to Appendix F. Table 1 shows the test error of our model compared against Deep Sets [47] and Set Transformer [27], two previous state-of-the-art architectures for sets. Our model achieves much lower **o.o.d** generalisation error than other methods, even lower than Deep Sets with a built-in Max-Pooling function.

Table 1: **o.o.d** generalisation test error for learning to find the maximum number in a set of numbers ($mean \pm std$ for 10 runs). M.S.E means Mean Squared Error.

Model	Deep Sets [47](Mean)	Deep Sets [47](Max)	Set Transformer [27]	OURS
M.S.E	73.22 ± 17.11	0.51 ± 0.29	1.62 ± 0.76	$\mathbf{0.0015 \pm 0.0008}$

3.2 Visual Object Comparison

For visual object comparison task, we set three sub-tasks for comparing different attributes of the object, including size, horizontal position and colour intensity. For each task we sample visual objects with different range for the compared attributes from dSprites dataset [20]. Given the compared attribute range $[V_{low}, V_{high}]$, we sample training data from range $[V_{low}, \frac{2}{3}V_{high})$ and test data from range $[\frac{2}{3}V_{high}, V_{high}]$. As ground truth attribute value is provided in dSprites dataset, we can build the comparison label as $(\mathbb{1}_{a_1<a_2}, \mathbb{1}_{a_1=a_2}, \mathbb{1}_{a_1>a_2})$. For all experiments we sample 60000 training pairs and 20000 test pairs. We test our proposed model against an MLP baseline, which directly processes the object representations o_i and o_j extracted by CNN as $MLP(o_i, o_j)$. We select the best MLP by hyper-parameter search over the number of layers and layer sizes. We use 1-dimensional projection as we find this gives the highest accuracy. Table 2 shows the **o.o.d** generalisation test accuracies of our model compared against the baseline. Our model with low-dimensional comparator significantly outperforms baselines for all three compared attributes.

Table 2: **o.o.d** generalisation test accuracies of baseline and our proposed model for dSprites attribute comparison task (10 runs). X-Coord is horizontal position.

Attributes / Model	Size	X-Coord	Colour
Baseline	$79.52 \pm 6.71\%$	$66.14 \pm 5.03\%$	$78.45 \pm 5.04\%$
OURS	$\mathbf{94.05 \pm 3.03\%}$	$\mathbf{79.11 \pm 1.92\%}$	$\mathbf{91.39 \pm 5.84\%}$

3.3 Visual Reasoning for Raven Progressive Matrices

For RPM-style task we use the extrapolation split of PGM dataset [4], which is already a well-defined **o.o.d** generalisation task. We compare our proposed model against all previous methods (to the best of our knowledge) that have reported results on the extrapolation data split. We additionally include a baseline model named "MLRN-P", which is a 2-layer MLRN [22] with prior knowledge of the relations only present in rows/columns and with pre-training. Table 3 shows the test accuracy comparison. Our proposed model outperforms all other baselines. We note that we used a vanilla CNN as the perception module, same as most previous methods [4, 48, 22] on RPM tasks. Multiple-object representation learning methods [16, 25, 42], which achieve better results for multi-object scene learning than CNN, can be investigated for potential improvement in generalisation performance. We leave this as future works.

Table 3: **o.o.d** generalisation test accuracies for the extrapolation split of PGM dataset.

Model	WReN [4]	MXGNet [43]	MLRN [22]	MLRN-P	OURS
Accuracy	17.2%	18.9%	14.9%	18.1%	**25.9%**

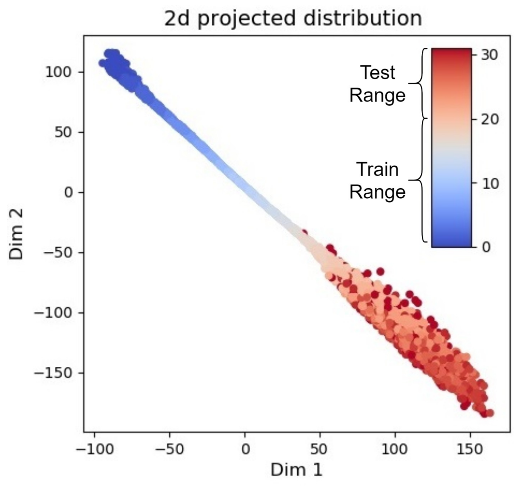

(a) 2D projection space

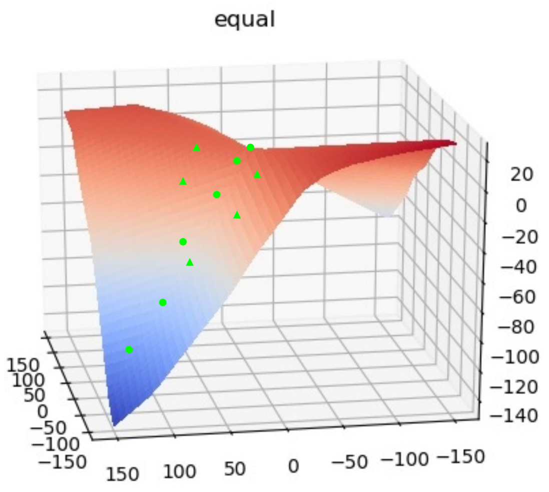

(b) 2D comparator function

Figure 4: (a) shows a scatter plot of the 2D projected distribution of objects in the task of comparing vertical positions of objects in the image. X-axis and Y-axis are 2 dimensions of the projection manifold. Latent vertical position (ranging from 0 to 32) is indicated by colour. (b) plots the comparator's function landscape for "equal" output unit (before softmax) in the space of vector differences between 2D projections of objects. Green circles represent vector difference sampled from training set while triangles represent vector difference sampled from test set.

3.4 Why Low Dimension?

While we show that comparator in low-dimensional manifolds improve **o.o.d** generalisation for a range of relational reasoning tasks, the reason behind it is still not clear. In this section we analyse the projection space and comparator function landscape of the visual object comparison task to shed light on this. We first state 3 observations invariant across different sub-tasks comparing different attributes:

1. *When the ground truth attribute can be represented in 1-dimensional manifold (such as vertical position), comparators in higher dimensions learn to project the object representation into 1-dimensional manifold.* Figure 4a illustrates this with a plot of projection distribution for the task of comparing vertical positions. It can be observed that even though the projection space is 2-dimensional, the projected points cluster around a line.

2. *The projection of rest data in the manifold is less clustered around the sub-manifold of attributes than that of training data.* This can be observed from Figure 4a, where the points projected from the test set are more spread out than from the training set. There is also less order in the distribution of test points, where points of noticeably different intensity appear next to each other.

3. *The function landscape becomes less defined outside of the sub-manifold.* Figure 4b plots the comparator function landscape for the "equal" ($\mathbb{1}_{a_1=a_2}$) output unit over the space of vector differences between 2D projected representation $p(o_2) - p(o_1)$. Green circles and triangles represent vector differences of sampled points from training and test set respectively. The equality function is well defined in the sub-manifold in which training points (circles) lie, peaking close to the $(0, 0)$ point. However, outside of the training points' sub-manifold, the function is more random, with a significant region with higher function value than at $(0, 0)$ point. Note that the vector differences of test points (triangles) may be in this region.

From the above observations, we conclude that when comparators are of higher dimension than the intrinsic dimension of compared attributes, the projection tends to lie in a sub-manifold of the same dimension as for the attributes, resulting in the comparator function to be only well defined in that manifold. However, the projection of test data tends to escape from this sub-manifold into the region where the comparator function is never trained on, resulting in incorrect prediction.

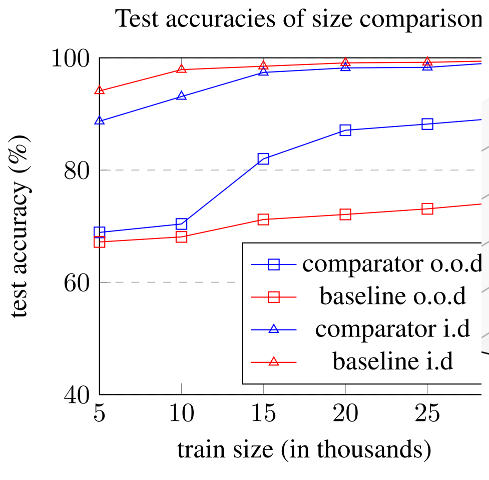

(a)

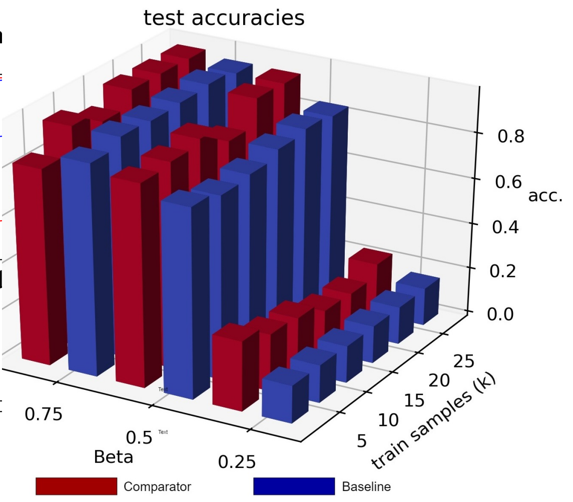

(b)

Figure 5: Figure (a) shows o.o.d and i.d. (identically distributed) test accuracy of baseline and comparator for different training sample sizes. (b) shows test accuracies of baseline and comparator for differnt training sample sizes and with different β-rate for truncating training distribution.

3.5 Algorithmic Alignment

Figure 5a shows the **o.o.d** and **i.d** (identically distributed) test accuracies for size comparison task of baseline and our proposed comparator model for different training sample sizes. It can be observed that **i.d** test accuracy's sample complexity (training samples needed to achieve the same accuracy), which measures algorithmic alignment, is not indicative of **o.o.d** test accuracies.

Figure 5b shows the size comparison of the test accuracies of baseline and comparator for different training sample sizes with different β rates for truncating the training distribution along the latent dimension 'size'. This corresponds to our proposed metric in Section 2.5. The new metric reflects that the model which learns better with truncated training distribution is the one with better **o.o.d** generalisation.

4 Related Work

o.o.d Generalisation: The deep neural network's lack of **o.o.d** generalisation (sometimes termed domain generalisation or extrapolation) capability has recently come under scrutiny. Different types of approaches have been proposed to improve **o.o.d** generalisation, such as reducing superficial domain specific statistics of training data [44, 8], adversarially learn representations that are domain-invariant [28, 1], disentangling representations to separate functional variables with spurious correlations [19, 15], and constructing models with innate causal inference graphs to reduce dependence on spurious correlations [3, 7]. Our work aligns more with the line of works on discovering inductive-bias that improves generalisation. Arguably CNN [26] is such an inductive-bias that improves generalisation on image datasets, and Graph Neural Network is an inductive-bias that improves generalisation on graph-structured data [5]. Trask et al [40] proposed Neural Arithmetic Logic Units (NALU), an inductive-bias that allows neural networks to learn simple arithmetic with improved **o.o.d** generalisation. Madsen et al [30] improves NALU for faster and more stable convergence.

Relational Reasoning: There is a wide range of relational reasoning tasks such as Visual Question Answering [2, 23], Raven Progressive Matrices [4, 48], Knowledge Base Query [34, 11] and Inferring Physical interactions [24, 35]. These tasks involve comparing entities such as visual objects to infer relations between them. A large proportion of models proposed to solve relational reasoning tasks fall into the broader range of graph neural networks and relational networks (see [5] for a comprehensive review). Our work is mostly orthogonal to these works, and may be viewed as a special type of edge layer that can be integrated into most of these models. There is another line of research on neural-symbolic models [46, 31], which use pre-defined programs to process extracted semi-symbolic object representations. Our work differs from these approaches in that our proposed model is not pre-defined to perform any functions, but learns to compare representations induced by the our proposed architecture.

Broader Impact

The generalisation capability of AI systems is a key factor affecting its applicability in industrial and daily scenarios. The system's lack of generalisation to unseen situations will lead to safety, security and financial risks. Examples includes autonomous driving vehicles not recognising unseen objects and crashing into them because this object has not been included in the training data. Our work aim to improve NN's generalisation ability for relational reasoning tasks, which are performed in many broader tasks such as autonomous driving and industrial component assembly. While our work is exploratory as we focus on abstract visual reasoning tasks, we believe future extensions of our work will help making applications of AI systems safer and more viable.

References

[1] I. Albuquerque, J. Monteiro, T. H. Falk, and I. Mitliagkas. Adversarial target-invariant representation learning for domain generalization. *arXiv preprint arXiv:1911.00804*, 2019.

[2] S. Antol, A. Agrawal, J. Lu, M. Mitchell, D. Batra, C. Lawrence Zitnick, and D. Parikh. Vqa: Visual question answering. In *Proceedings of the IEEE international conference on computer vision*, pages 2425–2433, 2015.

[3] M. Arjovsky, L. Bottou, I. Gulrajani, and D. Lopez-Paz. Invariant risk minimization. *arXiv preprint arXiv:1907.02893*, 2019.

[4] D. Barrett, F. Hill, A. Santoro, A. Morcos, and T. Lillicrap. Measuring abstract reasoning in neural networks. In *International Conference on Machine Learning*, pages 511–520, 2018.

[5] P. W. Battaglia, J. B. Hamrick, V. Bapst, A. Sanchez-Gonzalez, V. Zambaldi, M. Malinowski, A. Tacchetti, D. Raposo, A. Santoro, R. Faulkner, et al. Relational inductive biases, deep learning, and graph networks. *arXiv preprint arXiv:1806.01261*, 2018.

[6] Y. Belinkov and Y. Bisk. Synthetic and natural noise both break neural machine translation. In *International Conference on Learning Representations*, 2018. URL `https://openreview.net/forum?id=BJ8vJebC-`.

[7] Y. Bengio, T. Deleu, N. Rahaman, N. R. Ke, S. Lachapelle, O. Bilaniuk, A. Goyal, and C. Pal. A meta-transfer objective for learning to disentangle causal mechanisms. In *International Conference on Learning Representations*, 2020. URL `https://openreview.net/forum?id=ryxWIgBFPS`.

[8] F. M. Carlucci, A. D'Innocente, S. Bucci, B. Caputo, and T. Tommasi. Domain generalization by solving jigsaw puzzles. In *Proceedings of the IEEE Conference on Computer Vision and Pattern Recognition*, pages 2229–2238, 2019.

[9] M. V. Chafee. A scalar neural code for categories in parietal cortex: Representing cognitive variables as "more" or "less". *Neuron*, 77(1):7–9, 2013.

[10] F. Chollet. On the measure of intelligence, 2019.

[11] B. Dhingra, M. Zaheer, V. Balachandran, G. Neubig, R. Salakhutdinov, and W. W. Cohen. Differentiable reasoning over a virtual knowledge base. In *International Conference on Learning Representations*, 2020. URL `https://openreview.net/forum?id=SJxstlHFPH`.

[12] J. K. Fitzgerald, D. J. Freedman, A. Fanini, S. Bennur, J. I. Gold, and J. A. Assad. Biased associative representations in parietal cortex. *Neuron*, 77(1):180–191, 2013.

[13] R. Geirhos, C. R. Temme, J. Rauber, H. H. Schütt, M. Bethge, and F. A. Wichmann. Generalisation in humans and deep neural networks. In *Advances in Neural Information Processing Systems*, pages 7538–7550, 2018.

[14] M. Gong and T. Liu. Biased neural coding of feature-based attention in human brain. *bioRxiv*, page 688226, 2019.

[15] S. Gowal, C. Qin, P.-S. Huang, T. Cemgil, K. Dvijotham, T. Mann, and P. Kohli. Achieving robustness in the wild via adversarial mixing with disentangled representations. *arXiv preprint arXiv:1912.03192*, 2019.

[16] K. Greff, R. L. Kaufmann, R. Kabra, N. Watters, C. Burgess, D. Zoran, L. Matthey, M. Botvinick, and A. Lerchner. Multi-object representation learning with iterative variational inference. *arXiv preprint arXiv:1903.00450*, 2019.

[17] U. Güçlü and M. A. van Gerven. Deep neural networks reveal a gradient in the complexity of neural representations across the ventral stream. *Journal of Neuroscience*, 35(27):10005–10014, 2015.

[18] T. Hafting, M. Fyhn, S. Molden, M.-B. Moser, and E. I. Moser. Microstructure of a spatial map in the entorhinal cortex. *Nature*, 436(7052):801–806, 2005.

[19] C. Heinze-Deml and N. Meinshausen. Conditional variance penalties and domain shift robustness. *arXiv preprint arXiv:1710.11469*, 2017.

[20] I. Higgins, L. Matthey, A. Pal, C. Burgess, X. Glorot, M. Botvinick, S. Mohamed, and A. Lerchner. beta-vae: Learning basic visual concepts with a constrained variational framework. *Iclr*, 2 (5):6, 2017.

[21] D. H. Hubel and T. N. Wiesel. Receptive fields of single neurones in the cat's striate cortex. *The Journal of physiology*, 148(3):574–591, 1959.

[22] M. Jahrens and T. Martinetz. Solving raven's progressive matrices with multi-layer relation networks. *arXiv preprint arXiv:2003.11608*, 2020.

[23] J. Johnson, B. Hariharan, L. van der Maaten, L. Fei-Fei, C. Lawrence Zitnick, and R. Girshick. Clevr: A diagnostic dataset for compositional language and elementary visual reasoning. In *Proceedings of the IEEE Conference on Computer Vision and Pattern Recognition*, pages 2901–2910, 2017.

[24] T. Kipf, E. Fetaya, K.-C. Wang, M. Welling, and R. Zemel. Neural relational inference for interacting systems. *arXiv preprint arXiv:1802.04687*, 2018.

[25] A. Kosiorek, S. Sabour, Y. W. Teh, and G. E. Hinton. Stacked capsule autoencoders. In *Advances in Neural Information Processing Systems*, pages 15486–15496, 2019.

[26] Y. LeCun, Y. Bengio, et al. Convolutional networks for images, speech, and time series. *The handbook of brain theory and neural networks*, 3361(10):1995, 1995.

[27] J. Lee, Y. Lee, J. Kim, A. Kosiorek, S. Choi, and Y. W. Teh. Set transformer: A framework for attention-based permutation-invariant neural networks. In *International Conference on Machine Learning*, pages 3744–3753, 2019.

[28] D. Li, Y. Yang, Y.-Z. Song, and T. M. Hospedales. Deeper, broader and artier domain generalization. In *Proceedings of the IEEE international conference on computer vision*, pages 5542–5550, 2017.

[29] L. Liu, H. Jiang, P. He, W. Chen, X. Liu, J. Gao, and J. Han. On the variance of the adaptive learning rate and beyond. *arXiv preprint arXiv:1908.03265*, 2019.

[30] A. Madsen and A. R. Johansen. Neural arithmetic units. *arXiv preprint arXiv:2001.05016*, 2020.

[31] J. Mao, C. Gan, P. Kohli, J. B. Tenenbaum, and J. Wu. The neuro-symbolic concept learner: Interpreting scenes, words, and sentences from natural supervision. *arXiv preprint arXiv:1904.12584*, 2019.

[32] D. Maurer. How the baby learns to see: Donald o. hebb award lecture, canadian society for brain, behaviour, and cognitive science, ottawa, june 2015. *Canadian Journal of Experimental Psychology/Revue canadienne de psychologie expérimentale*, 70(3):195, 2016.

[33] B. Recht, R. Roelofs, L. Schmidt, and V. Shankar. Do imagenet classifiers generalize to imagenet? In *International Conference on Machine Learning*, pages 5389–5400, 2019.

[34] T. Rocktäschel and S. Riedel. End-to-end differentiable proving. In *Advances in Neural Information Processing Systems*, pages 3788–3800, 2017.

[35] A. Sanchez-Gonzalez, N. Heess, J. T. Springenberg, J. Merel, M. Riedmiller, R. Hadsell, and P. Battaglia. Graph networks as learnable physics engines for inference and control. *arXiv preprint arXiv:1806.01242*, 2018.

[36] A. Santoro, D. Raposo, D. G. Barrett, M. Malinowski, R. Pascanu, P. Battaglia, and T. Lillicrap. A simple neural network module for relational reasoning. In *Advances in neural information processing systems*, pages 4967–4976, 2017.

[37] E. S. Spelke and K. D. Kinzler. Core knowledge. *Developmental science*, 10(1):89–96, 2007.

[38] X. Steenbrugge, S. Leroux, T. Verbelen, and B. Dhoedt. Improving generalization for abstract reasoning tasks using disentangled feature representations. *arXiv preprint arXiv:1811.04784*, 2018.

[39] C. Summerfield, F. Luyckx, and H. Sheahan. Structure learning and the posterior parietal cortex. *Progress in neurobiology*, 184:101717, 2020.

[40] A. Trask, F. Hill, S. E. Reed, J. Rae, C. Dyer, and P. Blunsom. Neural arithmetic logic units. In *Advances in Neural Information Processing Systems*, pages 8035–8044, 2018.

[41] A. Vaswani, N. Shazeer, N. Parmar, J. Uszkoreit, L. Jones, A. N. Gomez, Ł. Kaiser, and I. Polosukhin. Attention is all you need. In *Advances in neural information processing systems*, pages 5998–6008, 2017.

[42] D. Wang, M. Jamnik, and P. Lio'. Unsupervised and interpretable scene discovery with discrete-attend-infer-repeat. In *ICML workshop on Self-Supervised Learning*, page 9pp, 2019. URL `https://arxiv.org/abs/1903.06581`.

[43] D. Wang, M. Jamnik, and P. Lio. Abstract diagrammatic reasoning with multiplex graph networks. In *International Conference on Learning Representations*, 2020. URL `https://openreview.net/forum?id=ByxQB1BKwH`.

[44] H. Wang, Z. He, Z. C. Lipton, and E. P. Xing. Learning robust representations by projecting superficial statistics out. *arXiv preprint arXiv:1903.06256*, 2019.

[45] K. Xu, J. Li, M. Zhang, S. S. Du, K. ichi Kawarabayashi, and S. Jegelka. What can neural networks reason about? In *International Conference on Learning Representations*, 2020. URL `https://openreview.net/forum?id=rJxbJeHFPS`.

[46] K. Yi, J. Wu, C. Gan, A. Torralba, P. Kohli, and J. Tenenbaum. Neural-symbolic vqa: Disentangling reasoning from vision and language understanding. In *Advances in Neural Information Processing Systems*, pages 1031–1042, 2018.

[47] M. Zaheer, S. Kottur, S. Ravanbakhsh, B. Poczos, R. R. Salakhutdinov, and A. J. Smola. Deep sets. In *Advances in neural information processing systems*, pages 3391–3401, 2017.

[48] C. Zhang, B. Jia, F. Gao, Y. Zhu, H. Lu, and S.-C. Zhu. Learning perceptual inference by contrasting. In *Advances in Neural Information Processing Systems*, pages 1073–1085, 2019.

A Maximum of a Set: Architecture configurations

The architecture for the maximum of a set task has three sub-modules, namely a comparator $f(x_i, x_j)$, a comparison summariser $e_i = MLP(\sum_{j=1}^{N} f(x_i, x_j))$ and a pooling function $\sum_{i=1}^{N} a(e_i)p(x_i)$. For comparator f, we set K, the number of parallel comparisons (Equantion 1 in the main paper) to be 1 because the scalar valued real numbers does not have multiple parallel attributes. We implement the projection function p as a single feed forward layer. We choose 1-dimensional comparison space as this gives the best result. The comparison function c takes the projected difference $p(x_i) - p(x_j)$ as input, and is implemented as a single feed forward layer with 1 output unit. The MLP in the comparison summariser is implemented as a 2-layer MLP of hidden-size $16 - 1$. In the pooling function, the attention function a is implemented as a softmax layer which normalise e_i across $i \in 1 \ldots N$.

B Visual Object Comparison: Dataset Generation

In sections we describe details of visual object comparison dataset. We sample images from the dSprites dataset [20] and generate comparison labels (categories include smaller than, equal to, greater than) from ground truth latent values provided in the dataset. For each image in the dSprites dataset, 5 ground truth attribute values are provided, which are shape "category", "size", "rotation angle", "horizontal position" and "vertical position". We add "colour" as the 6th attribute by randomly generating colour intensity value in the range [0.1,0.2,0.3,0.4,0.5,0.6,0.7,0.8,0.9,1.0] for each image. We multiply image pixel values with the colour intensity, and add the colour intensity value to the ground truth latent values.

Algorithm 1 shows the pseudo-code for generating the visual object comparison dataset. compare_attr indicates the object attribute to be compare for the task. We pick three different attributes for experiments, which are "size", "horizontal position" and "colour intensity". We set training attribute range to be the lower 60% while test attribute range to be the upper 40%.

```
Input: train_size, test_size, compare_attr
train_data = EmptyList()
test_data = EmptyList()
for split in {train,test} do
  for i = 1 to train_size do
    attr_range, attr_idx = attr_stats(compare_attr)
    if split == train then
      LO, HI = 0, 0.6
    else
      LO, HI = 0.6, 1.0
    end if
    sample_range = Truncate(attr_range, LO, HI)
    latent_values_A = SampleLatent(attr_idx, sample_range)
    latent_values_B = SampleLatent(attr_idx, sample_range)
    image_A = SampleImage(latent_values_A)
    image_B = SampleImage(latent_values_B)
    less_than = latent_values_A < latent_values_B
    equal = latent_values_A == latent_values_B
    greater_than = latent_values_A > latent_values_B
    label = Concat(less_than, equal, greater_than)
    if split == train then
      train_data ← (image_A,image_B,label)
    else
      test_data ← (image_A,image_B,label)
    end if
  end for
end for
```

Algorithm 1: Visual Object Comparison Dataset Generation

C Visual Object Comparison: Architecture Configurations

In this section we list detailed configuration of the architecture with low-dim comparator and the baseline architecture. The architecture with low-dim comparator is illustrated in figure 3a. The CNN module is a 4-layer CNN of filter number $32 - 32 - 64 - 64$ followed by a 2-layer MLP of hidden size $256 - 10$. Each CNN layer has stride value 2 and padding value 1. The output of each CNN is the object representation o_i of raw image input x_i. The projection module p is a single feed forward layer projecting to a space with dimension d. We use $d = 1$ for reporting results except the manifold analysis experiments in section 3.4. The comparator takes projected vector difference $p(o_i) - p(o_j)$ as input, and is implemented as a 2-layer MLP of size $h - 3$, where h is the hidden size and 3 is the output size (corresponding to 3 different output categories). We found that varying h in the range 4 to 32 has little effect on the performance. Hence we report performance with the $h = 4$ to reduce computational costs.

The baseline architecture uses the same CNN module as the architecture with low-dim comparator. The baseline model concatenates the CNN output o_i and o_j and feed the concatenated vector into a MLP. We performed hyper-parameter search of the MLP with number of layers ranging from 1 to 4, and with hidden unit sizes from 32 to 64. We found that $64 - 64 - 3$ is the best performing architecture.

D PGM Dataset

In this section we give a brief description of PGM dataset. For more details please refer to [4]. PGM contains 8 context panels and 8 answer panels. The 8 context panels for a 3×3 diagram matrix. One is asked to pick the answer the logically fit with the context panels. In PGM, logic relations can exist in both rows and columns of the diagram matrix. Figure 6a and 6b show two examples from the PGM dataset(Image courtesy [4]). The first example contains a 'Progression' relation of the number of objects across diagrams in columns. The second examples contains a 'XOR' relation of position of objects across diagrams in rows. The objects in PGM datasets have different attributes such as colour and size. In total five types of relations can be present in the task: $\{Progression, AND, OR, XOR, ConsistentUnion\}$.

E PGM Architecture Configurations

In this section we describe detailed configuration of the PGM architecture with low-dim comparators, and the baseline model MLRN-P, which is an augmented version of MLRN [22]. The descriptions here is supplementary to descriptions in section 2.4 of the main paper and figure 3b.

The CNN module is a 4-layer CNN of filter number $32 - 32 - 64 - 64$ followed by a 2-layer MLP of hidden size $256 - 128$. Each CNN layer has stride value 2 and padding value 1. The output of each CNN is the object representation o_i of raw image input x_i. Following [4] we attach to o_i a position tag to indicate its position in the diagram matrix. The tagged object representation is then projected onto $K = 512$ 1-dimensional manifold for parallel attribute comparison. Next we describe the comparator module f (equation 1. As shown in figure 3b, there two hierarchical projection comparison. For the first level, we found that implementing c as a simple vector difference module achieve best results, which means $c = p(o_i) - p(o_j)$. This reflects the fact that comparison between diagrams is directional, such as increase in number of objects from one diagram to the other. We implement g in equation 1 as a residual MLP of 4 layers with hidden size $2048 - 2048 - 2048 - 796$. The output from each pairwise comparison of diagrams in a row/column are concatenated to form the relation embedding for that row/column. For the second level we implement c as absolute difference, which means $c = |p(o_i) - p(o_j)|$. This works better because relation comparison is less directional. For example the difference between relation of increasing number of objects and relation of increasing sizes of objects should be the same when the compared diagram is swapped. For the second level we implement g as 3 layer MLP of hidden sizes $1024 - 512 - 1$, which directly output the predicted similarity score between two rows/columns. For predicting the correct answer candidate we follow [4] by applying a softmax function to scores produced by comparing each answer rows/columns with context row/columns to produce scores for each answer candidates. For meta-target prediction we sum all context row/column embedding and process it with a 3-layer MLP

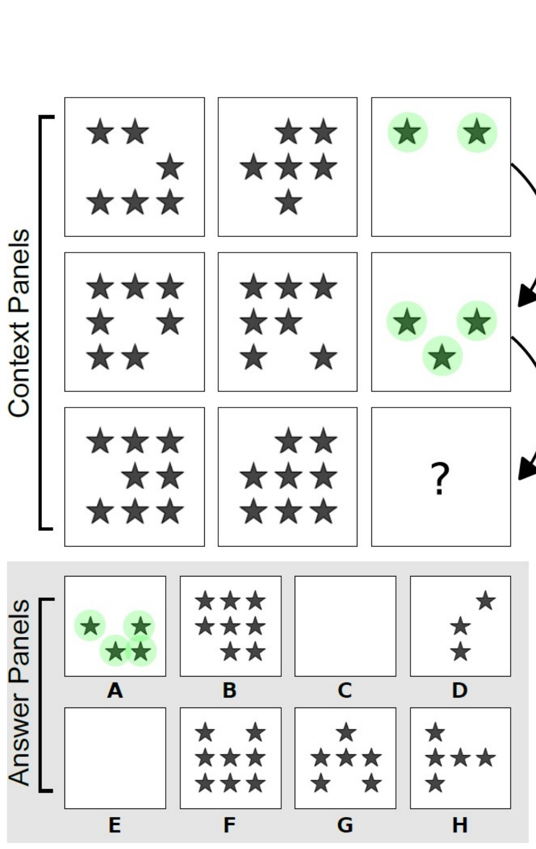

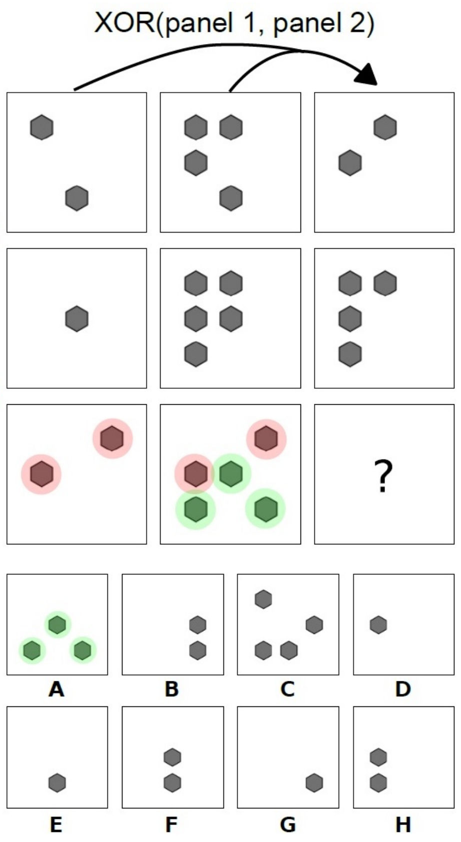

Figure 6: Two examples in PGM dataset. (a) task contains a 'Progression' relation of the number of objects across diagrams in columns while (b) contains a 'XOR' relation of position of objects across diagrams in rows. For both task "A" is the correct answer.

of hidden size $1024 - 512 - 12$, where 12 is the meta-target label size. We have attached source code in the submission for clarity.

The baseline model MLRN-P is modified from MLRN [22]. We have performed three architecture modifications for fair comparison with our model. Firstly we inject the prior knowledge of relations existing only in rows/columns into the model. The first level of Relation Networks compare diagrams within row/columns and the second level of Relation Networks compare row/colum embeddings. Secondly we swap MLP in the original MLRN with residual MLP, which is shown to improve performance slightly in our model. Thirdly we pretrained CNN module with Beta-VAE [20] for fair comparison with our model.

F Training Details

In this section we describe the training details for all three experiments. We use PyTorch[2] for implementation. For gradient descent optimiser, we use RAdam [29], an improved version of the Adam optimiser. For all 3 experiments we use learning rate 0.001 and betas (0.9,0.999). We used 2 Nvidia Geforce Titan Xp GPUs for training all models. For Maximum of a set and visual object comparison, we set batch size to be 64. For PGM we found a larger batch size of 512 slightly improves result. For Maximum of the set and visual object comparison we set training epochs to be 20. For PGM we trained for 50 epochs. For visual object comparison and RPM tasks we pre-trained

[2] `https://pytorch.org/`

CNN as the encoder of a Beta-VAE [20]. We follow standard training procedures of Beta-VAE as described in the paper, and set the β value to be 1.

G Additional Plots

In section 3.4 of the main paper we show plots of projected distribution and comparator's function landscape for position comparison task. In this section we show the same plots for comparison tasks for other attributes, which are sizes and colour intensity. Figure 7 shows the plot for size comparison while figure 8 shows the plot for colour intensity comparison. Training range is the lower 60% of the colour bar while test range is the upper 40%. The observations stated in section 3.4 also holds true for these attributes. For size and colour intensity comparison tasks, the projected distribution plots show that the test data is more clustered than that of spatial position comparison. This shows that size and colour intensity attributes can be learnt better with a bespoke CNN perception module than spatial position attributes. This is supported by that models trained for these two attributes achieved higher **o.o.d** test accuracies.

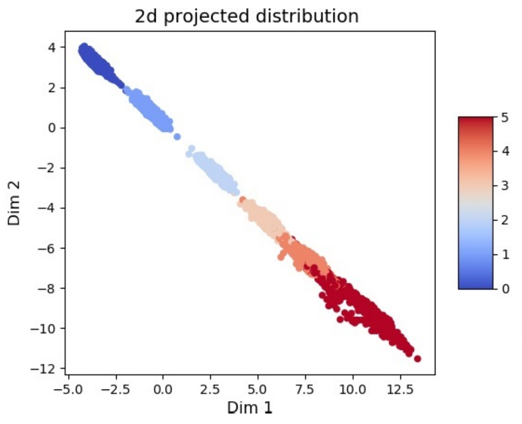

(a) 2D projection space

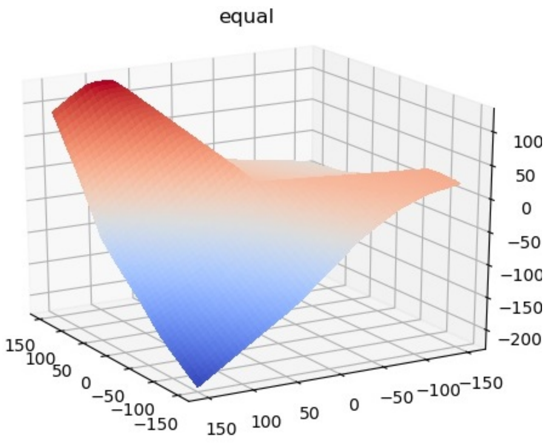

(b) 2D comparator function

Figure 7: (a) shows a scatter plot of the 2D projected distribution of objects in the task of comparing sizes of objects in the image. X-axis and Y-axis are 2 dimensions of the projection manifold. Latent size variable (possible values are [0,1,2,3,4,5]) is indicated by colour. (b) plots the comparator's function landscape for "equal" output unit (before softmax) in the space of vector differences between 2D projections of objects.

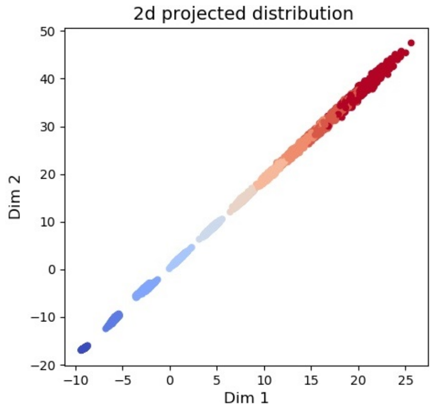

(a) 2D projection space

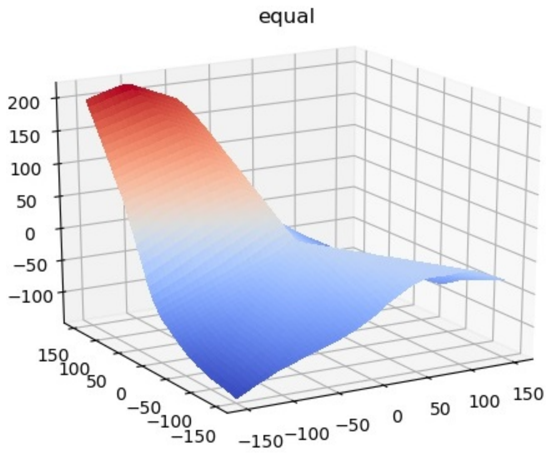

(b) 2D comparator function

Figure 8: (a) shows a scatter plot of the 2D projected distribution of objects in the task of comparing colour intensity of objects in the image. X-axis and Y-axis are 2 dimensions of the projection manifold. Latent colour intensity variable (possible values are [0.1,0.2,0.3,0.4,0.5,0.6,0.7,0.8,0.9,1.0]) is indicated by colour. (b) plots the comparator's function landscape for "equal" output unit (before softmax) in the space of vector differences between 2D projections of objects.